applied sciences

MDPI

Article

Laser Induced Nano and Micro Structures of Molybdenum Surface Applied in Multistage Depressed Collector for Secondary Electron Suppression

Jie Wang, Yong Gao, Zhiming You, Jiakun Fan, Jing Zhang, Sheng Wang * and Zhanglian Xu *

School of Energy and Power Engineering, Xi'an Jiaotong University, Xi'an 710049, China; wangjie1@xjtu.edu.cn (J.W.); gaoyong1108@stu.xjtu.edu.cn (Y.G.); youzm19960311@stu.xjtu.edu.cn (Z.Y.); inak960119@stu.xjtu.edu.cn (J.F.); zhangjing1108@stu.xjtu.edu.cn (J.Z.)

* Correspondence: shengwang@xjtu.edu.cn (S.W.); xuzhanglian@xjtu.edu.cn (Z.X.)

Received: 22 September 2019; Accepted: 15 October 2019; Published: 16 October 2019

check for updates

Abstract: The laser processing molybdenum metal surface method was first proposed to enhance the efficiency of multistage depressed collectors (MDCs). In this study, the secondary electron yield (SEY), surface geometrical morphologies and chemical states of laser processed Mo metal samples were characterized. For the first time, the effects of laser parameters and incident angle of primary electrons on the SEY property of laser induced nano and micro structures of molybdenum surface were investigated. The influence rule of laser processing patterns, power, pitch spacing, scanning speed on surface morphologies and SEY were systematically explored. A maximum SEY of laser processed Mo metal less than one was achieved. The Mo 3d and O 1s core level spectra of Mo metal before and after laser processing were analyzed in this study. Furthermore, the corresponding oxidation states of Mo as well as the relative distribution were elucidated.

Keywords: laser processing; Mo metal; secondary electron yield

1. Introduction

Traveling wave tube (TWT), a vital vacuum electronic device, has been widely used in satellite communications, radar, etc. [1–5]. The collector efficiency and beam wave interaction efficiency are the two major reasons for the efficiency enhancement of the TWT. The beam wave interaction efficiency is difficult to further enhance since it has reached a certain threshold value. Accordingly, improving collector efficiency will be the essential way for the efficiency improvement of the TWT. The multistage depressed collector, with the function of sorting and collecting interacted electrons based on the electron velocity, is commonly used to improve the collector efficiency. Secondary electron (SE) emission imposes on the working performance of multistage depressed collectors (MDCs), such as the change of collector efficiency, back-streaming rate, etc. Furthermore, the SEs will induce the heat dissipation power, additional noise power and the possible failure of the TWTs.

Previous studies demonstrated that MDC efficiency can be improved significantly with the secondary electron yield (SEY) of the inner surface of MDCs less than one [3,6]. In the earlier study [6], it was found that the maximum SEY ($\delta_{\mathbf{max}}$) of molybdenum masked ion-textured OFHC (oxygen-free high-conductivity copper) prepared by different ion-texturing parameters varied between 0.30 and 0.55 with the primary electron energy range of 200–2000 eV. M.Q. Ding et al. [7] demonstrated that the $\delta_{\mathbf{max}}$ of ion modified OFHC surface changed between 0.64 and 1.00 with the primary electron energy range of 100–1000 eV.

To improve the service behavior of MDCs, the conventional methods aim to optimize the electrode structure and the potential [8–11]. For example, Zhangliang Wang et al. proposed a novel non-axisymmetric structure MDC to achieve a low back-streaming rate and high collection efficiency with the advantage of easy processing and simple structure [12].

Besides, the suppression of secondary electron emission can also enhance the efficiency of the MDCs of vacuum electron devices. In order to reduce the emission of oxygen-free high-conductivity copper (OFHC), the most commonly used material for MDC electrodes, the ion texturing method [3,6,13] and various low SEY film coatings such as diamond-like carbon (DLC) [4] and TiC film coatings [14] were employed to obtain a low SEY OFHC surface. Mingqing Ding et al. studied the preparation and characterization of the molybdenum films deposition on MDC surfaces to reduce SEY of the MDCs surface and improve the total efficiency of TWTs [13]. After Mo deposited on the surface of the copper MDC substrate, the rough structures were formed with the low SEY property [13,14].

The laser induced nano- and micro-structures surface technique is an effective way to obtain a low SEY surface [15–17], with the advantage of ease of processing and excellent stability. Therefore, we proposed that laser treated Mo and copper with low SEY can serve as collector electrodes. The SEY properties of the laser treated OFHC have been studied in the previous literature [16]. Molybdenum was selected because of its higher melting temperature than that of copper and being compatible with furnace-brazing procedures commonly used in the fabrication of MDC and TWT. In this paper, the SEY, surface topography and surface composition of laser treated Mo were characterized and the correlation mechanism of SEY and surface topography were analyzed. Moreover, allium giganteum flower-like biomimetic structures with the property of capturing the secondary electrons based on the geometric effect were found to mainly contribute for the SEY decrease of laser processed Mo.

2. Experiments and Methods

2.1. Laser Parameters

Here, the preparation of bulk Mo samples with a purity of 97.96% was carried out by a fiber laser to produce nano/micro-structures surface at room temperature, as shown in Figure 1. Specifically, a K20-CS nanosecond pulsed fiber laser with a laser wavelength of 1064 nm was utilized for processing Mo samples with a dimension of 20.0 mm × 9.0 mm × 0.5 mm in an atmospheric environment. Mo samples were purchased from ELETM Company (Qingdao, China). Before SEY measurements, Mo samples were ultrasonically cleaned in acetone and absolute ethyl alcohol for 15 minutes, respectively.

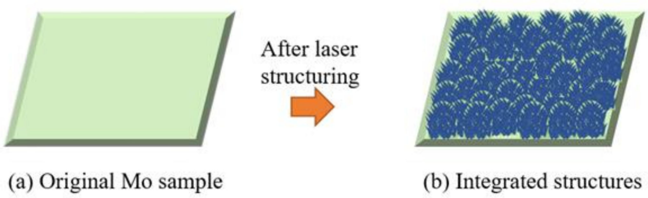

Figure 1. Schematic of the strategy for obtaining laser structured surfaces with a low secondary electron yield (SEY) property. (**a**) Original bulk Mo sample. (**b**) Integrated flocculent arrays formed after laser processing.

As listed in Table 1, low SEY laser processed Mo samples were fabricated by adjusting the laser average power, pitch spacing and scanning speed with cross and line hatched patterns. The $1/e^2$ diameter of spot size was about 15 µm. The focused length was 233 ± 0.1 mm. The pulse duration was 10 ns, with a repetition rate of 20 kHz, an average power of 10–13.3 W and a fluence per dose of 0.5 mJ at average power of 10 W. A scanner head was adopted to scan over the Mo samples which were fixed on the sample stage.

Table 1. Laser parameters of laser treated Mo samples. Here, δ_{max} is the maximum SEY within the certain primary electron energy range investigated (100–3000 eV in this study) and E_{max} is the primary electron energy corresponding to the maximum SEY.

Sample	Hatched Pattern	Average Power /W	Spot /μm	Pitch Spacing/μm	Scanning Speed /mm s^{-1}	δmax	*E*max /eV
#1	Cross	10	15	15	100	1.13	400
#2	Cross	10	15	15	1000	1.11	2400
#3	Line	10	15	15	100	0.96	1500
#4	Line	10	15	20	100	0.95	2000
#5	Line	10	15	15	1000	1.35	300
#6	Line	13.3	15	15	100	0.82	1200
#7	Line	13.3	15	15	1000	1.07	300

2.2. Characterization Method

A JEOL 7800F Schottky field SEM (scanning electron microscope) was used to conduct a systematic research on the influence of different laser parameters, such as average power, pitch spacing and scanning speed on surface geometrical morphology of laser processed Mo samples. The X-ray photoelectron spectroscopy (XPS) surveys were performed using an AXIS ULtrabld spectrometer with non-monochromatized Al Ka X-ray source operated at 150 W. The SEY testing equipment is introduced in detail in Reference [18]. With a primary electron (PE) dose of 7.6×10^{-6} C $\cdot$mm^{-2} and a PE current of 10 nA, the SEY of laser processed Mo metal samples was characterized using a dedicated SEY measurement set-up at the incident angles of 90°, 80° and 60°. Here, the incidence angle, θ, acted as the angle between the sample surface and the incident PEs.

3. Results and Discussion

Laser parameters, such as pitch spacing, hatch pattern, scanning speed etc., can influence the surface structures affecting the SEY characteristics of the Mo samples significantly. Thus, line and cross hatched patterns were adopted. When the laser scan speed was lower than 50 mm/s, the Mo sample was bended by laser visibly. The δ_{max} of laser treated Mo sample #5 with the scan speed of 1000 mm/s was 1.35, slightly lower than that of the untreated one. In order to improve the density of sphere/columnar/allium giganteum regel-like structures, the pitch spacing was usually equal to or slightly larger than the spot size. Next, the effect of processing patterns, average power, pitch spacings, scan speeds and incident angles on the SEY of laser treated Mo samples are discussed and analyzed in detail.

3.1. Processing Patterns

The SEY characterizations of untreated Mo (green curve), laser engineered Mo samples #1 (light blue curve), #2 (orange curve), #3 (crimson curve), #4 (pink curve), #5 (purple curve), #6 (dark blue curve) and #7 (fluorescent green curve) are shown in Figure 2. The δ_{max} of untreated Mo is 1.46 in this study, while the one of Mo samples reported by other researchers varied between 1.0–1.3 [19–22]. The SEY difference was associated with surface chemical states, primary electron doses, and so on.

Samples #1 and #3 were processed by the laser with the same laser parameters except for the hatched pattern and scanning speed. The cross hatched pattern was used for the laser processing of sample #1 and #2, while the line hatched pattern was for samples #3 and #5. The δ_{max} of sample #1, #2, #3 and #5 decreased from 1.46 to 1.13, 1.11, 0.96 and 1.35, compared with the one of non-treated Mo sample. At a low scanning speed (100 mm s^{-1}), the δ_{max} of sample #1 with the cross hatched pattern was higher than that of sample #3 with the line hatched pattern when the primary energy (E_p) ranged from 100 eV and 3000 eV. While, at a high scanning speed (1000 mm s^{-1}), the δ_{max} of sample #2 with cross hatched pattern was lower than that of sample #5 with the line hatched pattern at $E_p \leq 1800$ eV and higher at 1800 eV ≤ E_p ≤ 3000 eV. Therefore, with the SEY less than one at 100 eV ≤ E_p ≤ 3000 eV, the laser parameters of sample #3 were appropriate for secondary electron suppression.

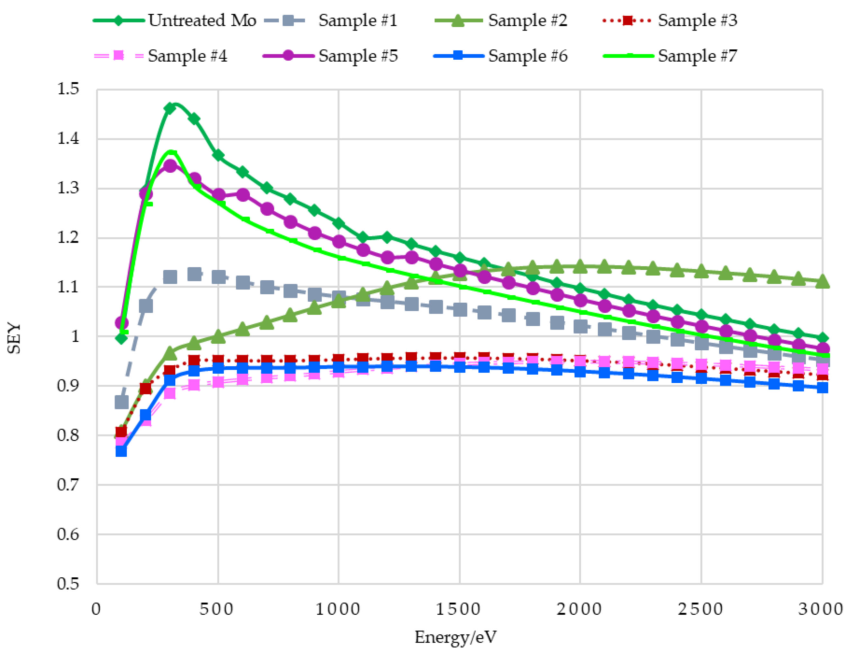

Figure 2. The SEY results of untreated Mo, laser processed Mo samples #1, #2, #3, #4, #5, #6 and #7. Sample #1 (cross hatched pattern), #3 (line hatched pattern) and #6 (line hatched pattern) were processed with the same scanning speed of 100 mm s^{-1}. Sample #2 (cross hatched pattern), #5 (line hatched pattern) and #7 (line hatched pattern) were processed by the same scanning speed of 1000 mm s^{-1}. Samples #1, #2, #3, #4 and #5 were treated with the same laser power of 10 W, while samples #6 and sample #7 were processed by the same laser power of 13.3 W. The pitch spacings of sample #1, #2, #3, #5, #6 and #7 were all 15 µm and the one of sample #4 was 20 µm. The other laser ablation parameters of these seven laser treated samples are shown in Table 1.

The surface topography images of samples #1, #2, #3 and #5 are shown in Figure 3. Figure 3(a2–g2) suggest that the special topographies of laser treated Mo were similar to the flower of allium giganteum regel. Because the repetition rate was 20 kHz and the scan speed was 1000 mm s^{-1}, the distance between two spots was 50 µm. Therefore, the distance of samples #2, #5 and #7 in the SEM micrographs was much larger than those of the others. Comparing to the δ_{max} of untreated Mo, the ones of samples #1, #2, #3 and #5 were lower. It was speculated that this kind of micro size allium giganteum regel like structures could to some extent capture the secondary electrons based on the geometric effect. However, the area of this special structure was part of the whole sample surface. Different laser parameters produced different area ratios of this allium giganteum regel like structure. Subsequently, the effect of this structure on SEY reduction varied with the laser ablation parameters.

Sample #1 was processed by a laser with a cross pattern, while the SEM micrograph of this sample in Figure 3(a1) shows the traces of the line hatched pattern. This can be explained by the finding that transverse processing traces were overlapped by the longitudinal traces at a relatively high average power and a low scanning speed. For sample #2 with the high laser scanning speed, the cross pattern was observed clearly.

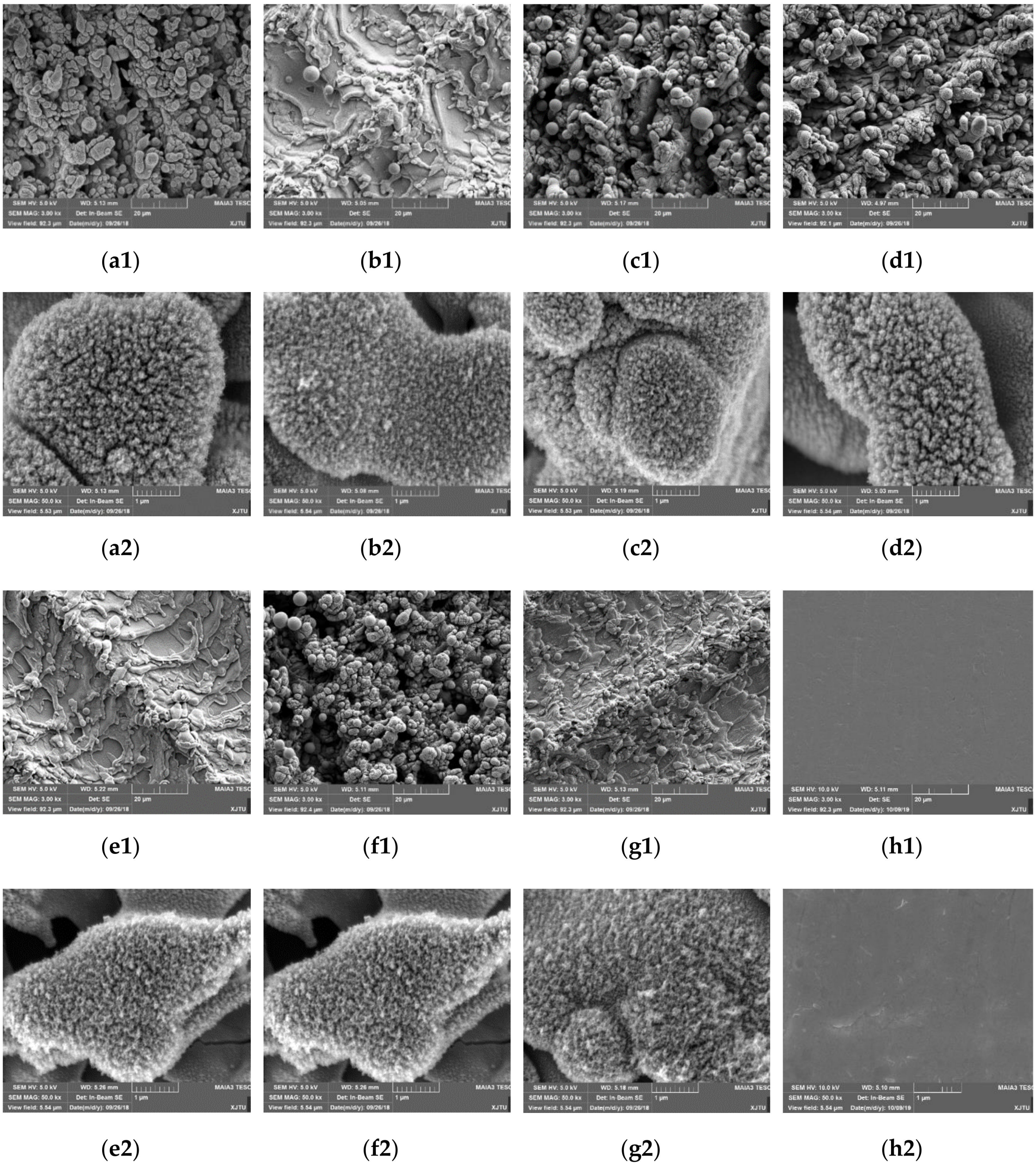

Figure 3. SEM images of untreated and laser processed Mo samples. (**a1**,**a2**) sample #1, (**b1**,**b2**) sample #2, (**c1**,**c2**) sample #3, (**d1**,**d2**) sample #4, (**e1**,**e2**) sample #5, (**f1**,**f2**) sample #6, (**g1**,**g2**) sample #7 and (**h1**,**h2**) untreated Mo samples. Samples #1 (cross hatched pattern), #3 (line hatched pattern) and #6 (line hatched pattern) were processed with the same scanning speed of 100 mm s^{-1}. Samples #2 (cross hatched pattern), #5 (line hatched pattern) and #7 (line hatched pattern) were processed by the same scanning speed of 1000 mm s^{-1}. Samples #1, #2, #3, #4 and #5 were treated with the same laser power of 10 W, while sample #6 and sample #7 were processed by the same laser power of 13.3 W. The pitch spacings of samples #1, #2, #3, #5, #6 and #7 were all 15 µm and the one of sample #4 was 20 µm. The other laser ablation parameters of these seven laser treated samples are shown in Table 1.

3.2. Average Power

The SEY characterization of the laser processed Mo samples #3 (crimson curve), #5 (purple curve), #6 (dark blue curve) and #7 (fluorescent green curve) with the line hatched pattern are shown in Figure 2. Samples #3 and #6 were processed by laser with the same laser parameters excluding the average power. The δ_{max} of samples #3, #5, #6 and #7 decreased from 1.46 to 0.96, 1.35, 0.82 and 1.07, compared to that of the non-treated Mo sample. When the scanning speeds of samples #3 and #6 were 100 mm s^{-1}, the shapes of the SEY curves for samples #3 with the average laser power of 10 W and #6 of 13.3 W were very similar. This case happened for sample #5 of 10 W and #7 of 13.3 W with the same laser scanning speed of 1000 mm s^{-1}. For samples #3 and #6, the SEYs of these two curves increased linearly at $E_p \leq 400$ eV and then flattened off at $500 \leq E_p \leq 3000$ eV gradually, as shown in Figure 2. While, the curves of samples #5 and #7 increased linearly at $E_p \leq 300$ eV and then decreased at $300 \leq E_p \leq 3000$ eV. The SEY curves of samples #3, #5, #6 and #7 suggested that the SEY curves of samples #3 and #6 decreased gradually and that of samples #5 and #7 declined to less than 0.98 or even below 0.5 at $E_p \geq 3000$ eV.

The surface topography images of samples #3, #5, #6 and #7 are shown in Figure 3. It can be seen that the surface topographies of samples #3 and #6 were all covered by sphere/column-like structures. However, the densities of sphere/column-like structures of samples #5 and #7 were lower than that of samples #3 and #6. This may be the major reason why the SEYs of samples #5 and #7 were higher than the ones of samples #3 and #6 in the perspective of the geometrical effect.

In the operation of a multistage depressed collector, the trajectories of the true secondaries and reflected primaries were significantly different. The true secondary electrons were suppressed by the depressed collector fields, while the reflected primary electrons streamed back to the tube and slow wave circuit. The secondary electron current collected here included the true secondary electrons (typically less than 50 eV) and reflected primary electrons which were inelastic and elastically scattered (typically larger than 50 eV) from the surface with the same energy as the primaries [21,23]. As indicated in Reference [23], the backscattering coefficient was the ratio of the number of inelastic and elastically scattered electrons with energy typically larger than 50 eV to the number of PEs. In most cases, the backscattering coefficient flattened off with the increase of PE energy for outgassed metals, such as Ni, Pt, Ta, etc., at $400 \leq E_p$. While the true secondary electrons yield decreased with the increase of PE energy, at $400 \leq E_p$.

3.3. Pitch Spacing

The SEY results and surface topography images of the laser processed Mo samples #3 (crimson curve) and #4 (pink curve) with the line hatched pattern are given in Figure 2, respectively. Samples #3 and #4 were processed by laser with the same laser parameters except for pitch spacing. The δ_{max} of samples #3 and #4 decreased from 1.46 to 0.96 and 0.95, comparing to the one of non-treated Mo sample. The values and shapes of the SEY curves for sample #3 with the pitch spacing of 15 µm and #4 of 20 µm were very similar. For samples #3 and #4, the SEYs of these two curves increased linearly at $E_p \leq 5$ 00 eV and then flattened off at 500 eV $\leq E_p \leq$ 3000 eV. It can be conjectured that the SEYs of samples #3 and #4 decreased slowly at $E_p \geq 3000$ eV.

The surface topography images of samples #3 and #4 are shown in Figure 3(c1,c2,d1,d2), respectively. It was suggested that the surface topographies of samples #3 and #4 were very similar, all covered by sphere/columnar-like structures. More specifically, the surface topographies of these two samples at a view field of 5.54 µm all looked like the flower of allium giganteum regel.

3.4. Scanning Speed

The SEY curves of the laser engineered Mo samples #1 (light blue curve), #2 (orange curve), #3 (crimson curve), #5 (purple curve), #6 (dark blue curve) and #7 (fluorescent green curve) are shown in Figure 2. Samples #1 and #2 were processed by laser with the same laser parameters except for laser scanning speed as the cross hatched pattern.

The δ_{max} of sample #1 (scanning speed of 100 mm s^{-1}) was higher than that of sample #2 (scanning speed of 1000 mm s^{-1}) at $E_p \leq 1400$ eV and lower than that of sample #2 at 1400 eV $\leq E_p \leq$ 3000 eV. However, the δ_{max} of sample #5 (scanning speed of 1000 mm s^{-1}) was above that of sample #3 (scanning speed of 100 mm s^{-1}) at $100 \leq E_p \leq 3000$ eV for the line hatched pattern. The situation was similar for samples #6 and #7. It was concluded that low scanning speed contributed to low SEY surface with the line hatched pattern. It was estimated that the SEY curves flattened off for samples #2, #3 and #6 and decreased gradually for samples #1, #5 and #7 at $E_p \geq 3000$ eV.

The surface topography images of samples #1, #2, #3, #5, #6 and #7 are shown in Figure 3. It can be seen that the surface topographies of laser processed Mo samples #1, #3 and #6 were like the flower of allium giganteum regel with the view field of 5.54 ± 0.01 nm. The aggregates composed of micro- and nano-particles contributed to the multimodal roughness of the laser processing Mo surface. The Mo metal underwent various stages of melting and solidifying with oxide layers formation with nanoparticles covering it. The oxide states of laser processed Mo samples was analyzed in the following section.

3.5. The Effect of Incidence Angle on SEY

Incident primary electrons can collide on the inner surface of a multistage depressed collector with different incident angles. Thus, the effect of incident angle on the SEYs of laser processed Mo metals is assessed and discussed for the first time.

The SEY of samples #2 (orange curve) and #6 (dark blue curve) at different incidence angles, e.g., 90°, 80° and 60°, respectively, as shown in Figure 4. With the decrease in the incident angle, the SEYs of sample #2 by the cross hatched pattern and sample #6 by the line hatched pattern increased at various degrees. For sample #2, the SEY curves at the incidence angles of 90° and 80° were basically the same at 100 eV $\leq E_p \leq$ 3000 eV. For sample #6, the SEY difference for the incident angle of 90° and 80° increased with the increase of PE energy. By comparing it with the SEY at an incident angle of 90°, the ones with a 60° angle increased by about 0.03–0.14. As the SEY theory predicted, the normalized yield (δ/δ_{max}) varied as 1/cos(90°-θ), where δ_{max} denotes the maximum SEY at a normal incidence [21]. Therefore, the SEY of laser processed Mo increased with the decrease of the incident angle, which is consistent with reported references [24–27].

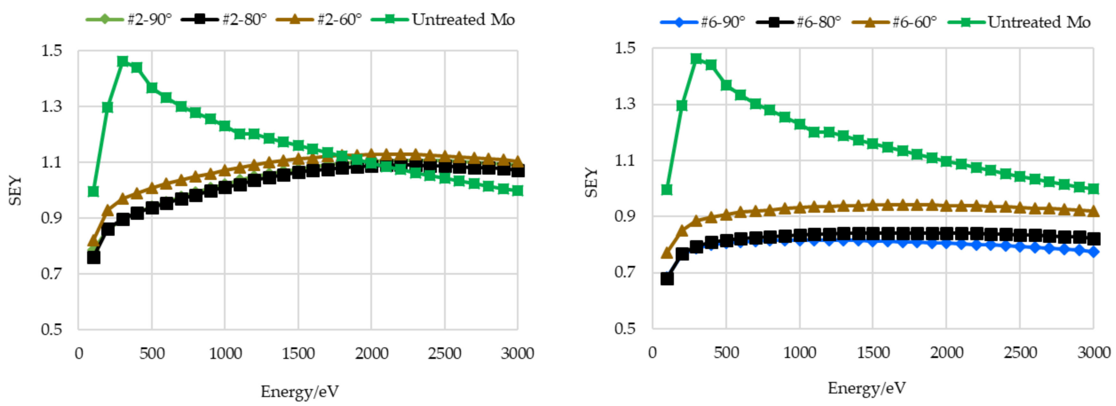

(**a**) (**b**)

Figure 4. The SEY curves of (**a**) sample #2 and (**b**) sample #6 at different incidence angles (90°, 80° and 60°, respectively) of primary electrons (Pes).

Compared to the previous studies [6,7], the δ_{max} of molybdenum masked ion-textured OFHC and ion modified OFHC varied between 0.30 and 1.00. In this study, the minimum δ_{max} of laser processed molybdenum ranging between 0.80 and 0.93 was obtained at different incident angles. The results indicated that a laser processed molybdenum surface is an effective way for the SE mitigation in MDCs, which should be considered for the application of the efficiency improvement of MDCs.

3.6. Chemical Analysis

The surface chemical circumstance is one of the key factors affecting the SEY of the surfaces. Therefore, XPS analysis was adopted to inquire into the chemical states of the surface elements. On the basis of the survey, scan spectra of untreated Mo and laser processed Mo sample #4 (Figure 5) showed that Mo, C, N and O were the dominant elements on the sample surfaces. The element ratios (At%) of Mo, C, N and O for untreated Mo and laser processed Mo were 12.7%:29.2%:32.2%:25.9% and 10.2%:37.3%:27.1%:25.4%, respectively. After laser processing, the atom ratios of Mo and N decreased slightly by about 2.5% and 5.1%, respectively. While, the atom ratio of C increased by about 8.1%, which may have been caused by the introduction of increased carbon impurity with the increases of the surface area. The element ratios of the O element basically remained unchanged before and after laser processing.

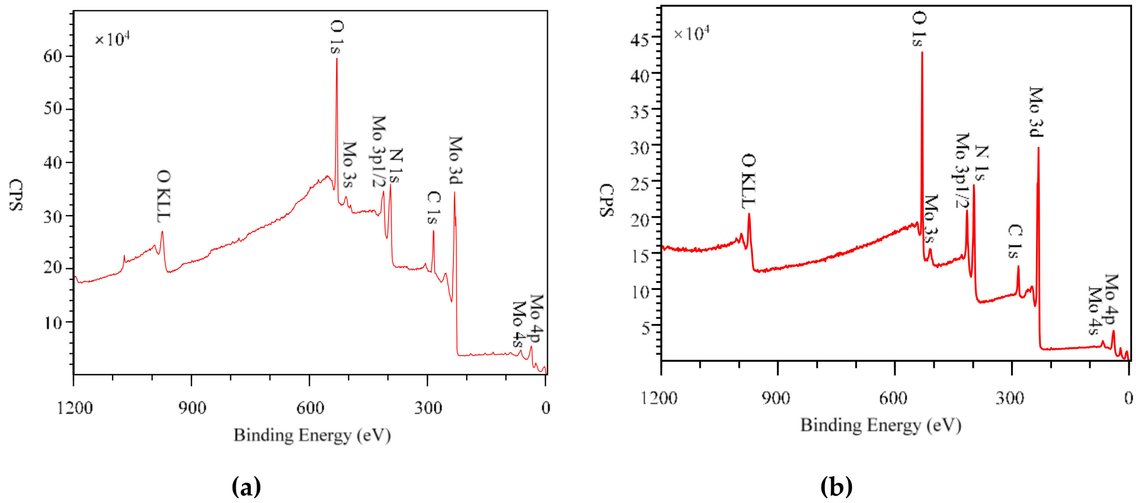

Figure 5. X-ray photoelectron spectroscopy (XPS) spectra of (**a**) untreated Mo and (**b**) laser treated Mo sample #4.

Spectra of the untreated Mo and laser treated Mo sample #4 with δ_{max} less than one are shown in Figure 6. The doublet peaks of 235.59 eV and 232.45 eV in terms of Mo-3d3/2 and Mo-3d5/2 were attributed to the Mo-3d spin-orbit splitting, which was consistent with the values in other references [28–30]. Gaussian 70%–Lorentzian 30% was used for deconvolution of the XPS peak for Mo and oxygen.

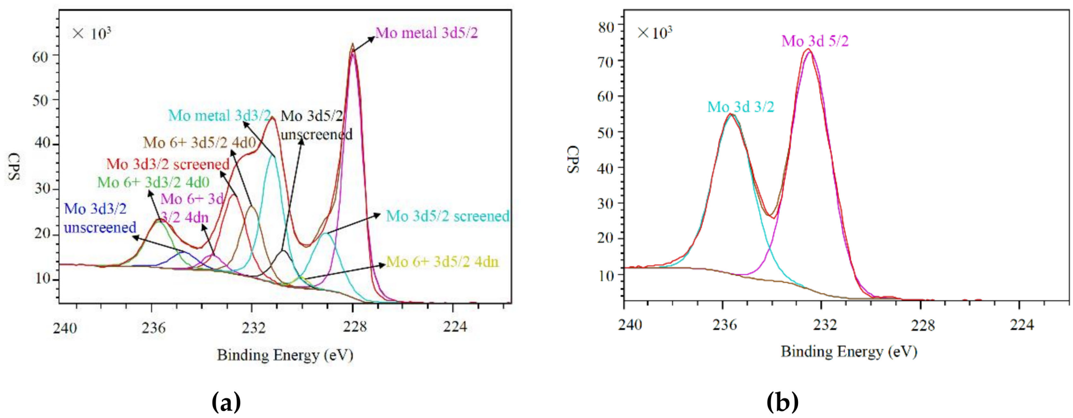

Figure 6. XPS core-level spectra of molybdenum (Mo-3d) for (**a**) untreated Mo and (**b**) laser treated Mo.

As discussed in refences [31,32], screened refers to the components at low binding energy due to well screened final states in which the localized level becomes occupied by an itinerant conduction electron. Besides, the unscreened is referred to as the broader components at higher binding energy associated with unscreened final states, in which the localized level remains empty. This demonstrated that the chemical state of laser treated Mo sample surface was Mo6+. The Mo-3d spectrum of untreated Mo in Figure 6a indicated that the content of Mo metal, Mo4+ and Mo6+ were 48.54%, 30.53% and 20.93%, respectively. The parameters for the Mo-3d spectra curve fitted of untreated Mo were consistent with those of Reference [33]. The surface of untreated Mo metal showed a relatively high level of original Mo metal with a value of 48.54%, while that of the laser treated Mo sample #4 showed the chemical state was Mo6+ which was dominated by a spin-orbit doublet. The Mo 3d spectrum of untreated Mo metal surface indicated that the chemical states of Mo were much more complex and consisted of Mo metal, MoO_2 along with spin-orbit doublet of MoO_3. The chemical states of the Mo element of untreated Mo sample were complicated, which included Mo metal and molybdenum oxide at different valence states. After laser processing in the atmosphere, the molybdenum sample surface was completely oxidized with the chemical state of Mo6+.

The characteristic peak positions for the O 1s state of untreated Mo and laser treated Mo sample #4 are presented in Figure 7. The O 1s spectrum of untreated Mo metal demonstrated that the percentages of O 1s-lattice oxide, O 1s-hydroxides and defect oxides, and O 1s-water and organic O were 31.71%, 50.06% and 18.23%, respectively. The concentrations of O 1s-lattice oxide, O 1s-hydroxides and defect oxides, and O 1s-water and organic O of laser treated Mo sample #4 were 73.67%, 24.92% and 1.41%, respectively. After laser processing, the percentage of O 1s-lattice oxide increased from 31.71% to 73.67%. Thus, stoichiometric formulation was formed on the surface of laser treated Mo metal. The metal oxides were almost always strong secondary emitters. However, many factors, such as surface oxidation states, surface morphology, surface roughness, etc., can affect the SEY of metal samples. In this paper, the laser ablation method was used to modify the surface morphology to form a low SEY surface (less than one). In subsequent studies, the laser ablation processing was performed in a vacuum or in an inert atmosphere. Moreover, the SEY difference of the same metal samples which were processed under different atmosphere will be compared and analyzed in the future.

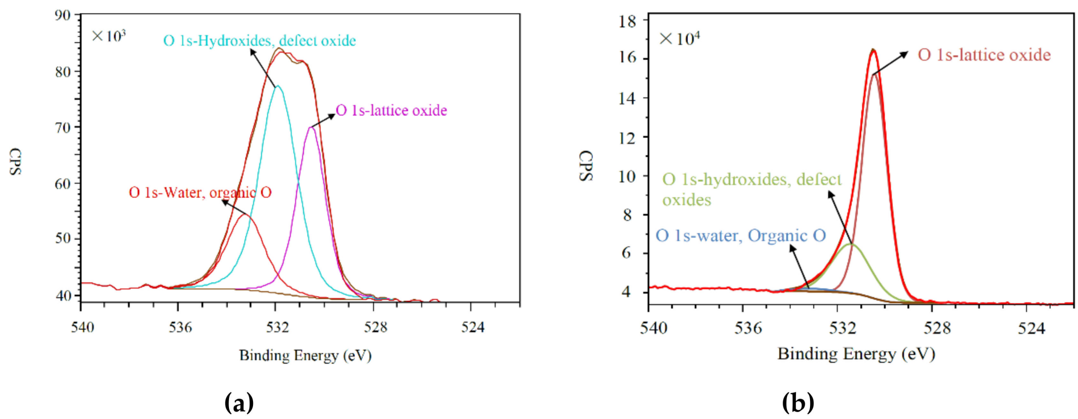

Figure 7. XPS core-level spectra of molybdenum (O-1s) for (**a**) untreated Mo and (**b**) laser treated Mo sample #4.

Geometry and surface chemical states change effects were the two main reasons for the SEY reduction of laser processed Mo metal. Previous studies demonstrated that the geometry effect was the main reason for SEY reduction [34,35]. The earlier studies [16,36] indicated that the oxidation states of laser treated copper was in terms of the SEY increase. Reference [22] investigated the SEY curves of dozens of metals before and after cleaning, which demonstrated that the surface oxidation can induce a SEY increase of 0.2~0.5. However, surface morphology was also an important factor affecting the SEY values. After laser processing, the Mo metal on the surface of the untreated Mo sample was almost fully oxidized. Although, Mo oxidation may have contributed to the SEY increase. While, laser induced nano- and micro-structures reduced the SEY. The balance effect was the SEY reduction of Mo samples. Thus, the degree of the contribution of surface chemical states changed on the reduction of SEY was not clear and requires further investigations.

As reported in references [9,10], the electron energy in MDC varied between 2 keV–24 keV, which may bombard on the inner surface of the MDC. When these electrons with the energy of 2 keV–24 keV impacted the inner surface of the MDC, the secondary electrons and backscattering electrons emitted formed the surface with the energy of 1 eV–24 keV, then part of the scattering electrons interacted with the inner surface and the beam in MDC. At 2000 eV $\leq E_p \leq$ 3000 eV, the SEY of untreated Mo ranged from 1.07 and 1.0. The SEY of sample #6 was 0.77~0.94 at 2000 eV $\leq E_p \leq$ 3000 eV with the incident angles of 90°, 80° and 60°, which was the lowest one in this study. Moreover, at 100 eV $\leq E_p \leq$ 2000 eV, the SEYs of sample #6 were less than one. Therefore, the laser processing parameters of sample 6 was preferable for SE mitigation in MDC.

4. Conclusions

Based on the requirements of enhancing the efficiency of MDC of the vacuum electron devices, the laser treated Mo metal collector method was proposed in this paper for the first time.

The XPS data found, provided valuable insights into changes induced by laser processing. The XPS chemical analysis results showed that the chemical states for the Mo 3d spectrum of laser treated Mo metal indicated the presence of Mo6+ which was in agreement with the reported literature. By comparing the Mo metal concentration of the untreated Mo sample and the laser treated Mo sample #4, Mo metal was nearly oxidized completely after laser processing.

It was speculated that these micro size allium giganteum regel like structures can, to some extent, capture the secondary electrons based on the geometric effect. However, the area ratio of this special structure varied with different laser parameters. Thus, the effect of this structure on SEY reduction varied with the laser ablation parameters.

After laser ablation, the laser treated Mo sample with the SEY less than one was obtained at 100 eV $\leq E_p \leq$ 3000 eV. The laser parameters of laser processed Mo sample #3, #4 and #6 were appropriate for secondary electron suppression. The SEY results of sample #6 at the incident angles of 90°, 80°, and 60°, respectively, were all less than one, which is more preferable for SEY reduction. The laser processing method was proved as a feasible way to obtain a low SEY Mo surface. The corresponding experimental verification of the laser processing Mo method to further improve the efficiency of MDC will be performed in the future.

Author Contributions: Conceptualization, J.W.; methodology, Z.Y., J.F. and J.Z.; validation, J.W. and Y.G.; investigation, J.W. and Y.G.; data curation, J.W., Y.G., Z.Y., J.F. and J.Z.; writing—original draft preparation, J.W.; writing—review and editing, J.W., S.W. and Z.X.; supervision, S.W. and Z.X.; funding acquisition, S.W. and Z.X..

Funding: This research was funded by the key project of Intergovernmental International Scientific and Technological Innovation Cooperation in China under Grant No. 2016YFE0128900, China Postdoctoral Science Foundation Grant No. 2018M643667, the Fundamental Research Funds for the Central Universities No. XJH012019018, the National Natural Science Foundation for the Youth of China No. 11905170, Shaanxi Province Postdoctoral Science Foundation Grant No. 2018104, the Fundamental Research Funds for the Central Universities No. XJH012019011, and the National Natural Science Foundation of China under Grant No.11775166.

Acknowledgments: We would like to thank Shengli Wu and Jie Li from the Institute of Physical Electronics and Devices of Xi'an Jiaotong University for their help with the SEY tests.

Conflicts of Interest: The authors declare no conflicts of interest.

References

1. Wu, C.; Pagonakis, I.G.; Illy, S.; Gantenbein, G.; Jelonnek, J. 3D simulation of a realistic multistage depressed collector for high-power fusion gyrotrons. In Proceedings of the 2016 IEEE International Vacuum Electronics Conference (IVEC), Monterey, CA, USA, 19–21 April 2016; pp. 16–17.

2. Wu, C.; Pagonakis, I.G.; Illy, S.; Thumm, M.; Gantenbein, G.; Jelonnek, J. Preliminary studies on multistage depressed collectors for fusion gyrotrons. In Proceedings of the 2016 German Microwave Conference (GeMiC), Bochum, Germany, 14–16 March 2016; pp. 365–368.
3. Curren, A.N.; Long, K.J.; Jensen, K.A.; Roman, R.F. An effective secondary electron emission suppression treatment for copper MDC electrodes. In Proceedings of the IEEE International Electron Devices Meeting, Washington, DC, USA, 5–8 December 1993; pp. 777–780.
4. Kussmaul, M.; Mirtich, M.J.; Curren, A.N. Ion beam treatment of potential space materials at the NASA Lewis Research Center. *Surf. Coat. Technol.* **1992**, *51*, 299–306. [CrossRef]
5. Ramins, P. Performance of computer designed small-size multistage depressed collectors for a high-perveance traveling wave tube. *NASA Tech. Pap.* **1984**, *2248*, 1–21.
6. Kenneth, A.; Curren, A.N.; Jensen, A.; Roman, R.F. Secondary emission electron characteristics of molybdenum-masked, ion-textured OFHC Copper. *NASA Tech. Pap.* **1990**, *2967*, 1–12.
7. Ding, M.Q.; Huang, M.G.; Feng, J.J.; Bai, G.D.; Yan, T.C. Ion surface modification for space TWT multistage depressed collectors. *Appl. Surf. Sci.* **2008**, *255*, 2196–2199. [CrossRef]
8. Huang, T.; Cao, Q.; Liu, J.; Gong, D.; Li, S.; Yang, Z.; Li, B. A multistage depressed collectors design tool for traveling wave tubes based on non-dominated sorting genetic algorithm II. In Proceedings of the 2018 IEEE International Vacuum Electronics Conference (IVEC), Monterey, CA, USA, 24–26 April 2018; pp. 175–176.
9. Mistry, C.; Chakraborty, S.; Arya, S.; Latha, A.M.; Roy, A.; Ghosh, S.K. A Study of Thermal Behavior of Travelling Wave Tube. In Proceedings of the 2018 IEEE International Vacuum Electronics Conference (IVEC), Monterey, CA, USA, 24–26 April 2018; pp. 133–134.
10. Pagonakis, I.G.; Wul, C.; Ell, B.; Avramidis, K.A.; Gantenbein, G.; Illy, S.; Thumm, M.; Jelonnek, J. Progress in the development of a multistage depressed collector system for high power gyrotrons. In Proceedings of the 2018 43rd International Conference on Infrared, Millimeter, and Terahertz Waves (IRMMW-THz), Nagoya, Japan, 9–14 September 2018.
11. Glyavin, M.; Manuilov, V.; Morozkin, M. Two-stage Energy Recovery System for DEMO Gyrotron. In Proceedings of the 2018 43rd International Conference on Infrared, Millimeter, and Terahertz Waves (IRMMW-THz), Nagoya, Japan, 9–14 September 2018.
12. Wang, Z.; Xu, X.; Gong, Y.; Duan, Z.; Wei, Y.; Gong, H.; Liu, H. A non-axisymmetric structure multistage depressed collector for sheet beam VEDs. In Proceedings of the 2017 Progress in Electromagnetics Research Symposium-Fall (PIERS-FALL), Singapore, 19–22 November 2017; pp. 403–407.
13. Mingqin, D.; Mingsuang, H.; Jinjun, F.; Guodong, B.; Xinghuil, L.; Qingping, Z.; Minghuil, L.; Yujuan, G.; Qilue, C. Secondary electron emission suppression of multistage vacuum depressed collector in space traveling tube by Mo ion deposition. *Chin. J. Vac. Sci. Technol.* **2009**, *3*, 247–250.
14. James, J.; Dayton, A. A review of the suppression of secondary electron emission from the electrodes of multistage collectors. In Proceedings of the ISDEIV. 18th International Symposium on Discharges and Electrical Insulation in Vacuum (Cat. No. 98CH36073), Eindhoven, The Netherlands, 17–21 August 1998; pp. 9–15.
15. Valizadeh, R.; Malyshev, O.B.; Wang, S.; Zolotovskaya, S.A.; Gillespie, W.A.; Abdolvand, A. Low secondary electron yield engineered surface for electron cloud mitigation. *Appl. Phys. Lett.* **2014**, *105*, 231605. [CrossRef]
16. Wang, J.; Sian, T.; Valizadeh, R.; Wang, Y.; Wang, S. The effect of air exposure on SEY and surface composition of laser treated copper applied in accelerators. *IEEE Trans. Nucl. Sci.* **2018**, *65*, 2620–2627. [CrossRef]
17. Watts, C.; Gilmore, M.; Schamiloglu, E. Effects of laser surface modification on secondary electron emission of copper. *IEEE Trans. Plasma. Sci.* **2011**, *39*, 836–841. [CrossRef]
18. Wang, J.; Gao, Y.; Fan, J.; You, Z.; Wang, S.; Xu, Z. Study on the effect of laser parameters on the SEY of aluminum alloy. *IEEE Trans. Nucl. Sci.* **2019**, *66*, 609–615. [CrossRef]
19. Dekker, A.J. Secondary electron emission. In *Solid State Physics*; Academic Press: Cambridge, MA, USA, 1958; Volume 6, pp. 251–331.
20. Lin, Y.; Joy, D.C. A new examination of secondary electron yield data. *Surf. Interface Anal.* **2005**, *37*, 895–900. [CrossRef]
21. Seiler, H. Secondary electron emission in the scanning electron microscope. *J. Appl. Phys.* **1983**, *54*, R1–R18. [CrossRef]

22. Walker, C.G.H.; El-Gomati, M.M.; Assa'D, A.M.D.; Zadrazil, M. The secondary electron emission yield for 24 solid elements excited by primary electrons in the range 250–5000 eV: A theory/experiment comparison. *Scanning* **2008**, *30*, 365–380. [CrossRef] [PubMed]
23. Thomas, S.; Pattinson, E.B. Automatic measurement of secondary electron emission characteristics of TaC, TiC and ZrC. *J. Phys. D Appl. Phys.* **1969**, *2*, 1539–1547. [CrossRef]
24. Svensson, B.; Holmén, G.; Burén, A. Angular dependence of the ion-induced secondary-electron yield from solids. *Phys. Rev. B* **1981**, *24*, 3749–3755. [CrossRef]
25. Thieberger, P.; Hanson, A.L.; Steski, D.B.; Zajic, V.; Zhang, S.Y.; Ludewig, H. Secondary-electron yields and their dependence on the angle of incidence on stainless-steel surfaces for three energetic ion beams. *Phys. Rev. A* **2000**, *61*, 042901. [CrossRef]
26. Kirby, R.E.; King, F.K. Secondary electron emission yields from PEP-II accelerator materials. *Nucl. Instrum. Methods Phys. Res. Sect. A* **2001**, *469*, 1–12. [CrossRef]
27. Balcon, N.; Payan, D.; Belhaj, M.; Tondu, T.; Inguimbert, V. Secondary electron emission on space materials: Evaluation of the total secondary electron yield from surface potential measurements. *IEEE Trans. Plasma Sci.* **2012**, *40*, 282–290. [CrossRef]
28. Belanger, D.; Laperriere, G. Electrochromic Molybdenum Trioxide thin film preparation and characterization. *Chem. Mater.* **1990**, *2*, 484–486. [CrossRef]
29. Guerfi, A.; Paynter, R.W.; Dao, H. Characterization and stability of electrochromic MoO3 thin films prepared by electrodeposition. *J. Electrochem. Soc.* **1995**, *142*, 3457–3464. [CrossRef]
30. Sivakumar, R.; Gopinath, C.S.; Jayachandran, M.; Sanjeeviraja, C. An electrochromic device (ECD) cell characterization on electron beam evaporated MoO_3 films by intercalating/deintercalating the H+ ions. *Curr. Appl. Phys.* **2007**, *7*, 76–86. [CrossRef]
31. Campagna, M.; Wertheim, G.K.; Shanks, H.R.; Zumsteg, F.; Banks, E. Local character of many-body effects in X-ray photoemission from transition-metal compounds: NaxWO3. *Phys. Rev. Lett.* **1975**, *34*, 738–741. [CrossRef]
32. Wertheim, G.K.; Kufner, S. Many-body line shape in x-ray photoemission from metals. *Phys. Rev. Lett.* **1975**, *35*, 53–56. [CrossRef]
33. Scanlon, D.O.; Watson, G.W.; Payne, D.J.; Atkinson, G.R.; Egdell, R.G.; Law, D.S.L. Theoretical and Experimental Study of the Electronic Structures of MoO3 and MoO2. *J. Phys. Chem. C* **2010**, *114*, 4636–4645. [CrossRef]
34. Valizadeh, R.; Malyshev, O.B.; Wang, S.; Sian, T.; Gurran, L.; Goudket, P.; Cropper, M.D.; Sykes, N. Low secondary electron yield of laser treated surfaces of copper, aluminium and stainless steel. In Proceedings of the 7th International Particle Accelerator Conference (IPAC'16), Busan, Korea, 1 June 2016; pp. 1089–1092.
35. Valizadeh, R.; Malyshev, O.B.; Wang, S.; Sian, T.; Cropper, M.D.; Sykes, N. Reduction of secondary electron yield for E-cloud mitigation by laser ablation surface engineering. *Appl. Surf. Sci.* **2017**, *404*, 370–379. [CrossRef]
36. Yamamoto, K.; Shibata, T.; Ogiwara, N.; Kinsho, M. Secondary electron emission yields from the J-PARC RCS vacuum components. *Vacuum* **2007**, *81*, 788–792. [CrossRef]